A&A 603, A47 (2017)
DOI: 10.1051/0004-6361/201730800

Astronomy & Astrophysics

Neglected X-ray discovered polars

I. Giant flares in V358 Aquarii

K. Beuermann[1], V. Burwitz[2], K. Reinsch[1], A. Schwope[3], and H.-C. Thomas[4,⋆]

[1] Georg-August-Universität Göttingen, Institut für Astrophysik, Friedrich-Hund-Platz 1, 37077 Göttingen, Germany
e-mail: k.beuermann@t-online.de
[2] MPI für extraterrestrische Physik, Giessenbachstr. 6, 85740 Garching, Germany
[3] Leibniz-Institut für Astrophysik Potsdam (AIP), An der Sternwarte 16, 14482 Potsdam, Germany
[4] MPI für Astrophysik, Karl-Schwarzschild-Str. 1, 85740 Garching, Germany

Received 16 March 2017 / Accepted 13 April 2017

ABSTRACT

We report photometric and spectroscopic observations of the polar V358 Aqr (=RX J2316-0527) collected over 25 yr. It was discovered as a bright very soft X-ray source in the ROSAT All Sky Survey, but had lapsed into a low state when reobserved in 1993. We have obtained an optical photometric ephemeris, which is free of cycle count errors and allows to correctly phase events around the orbit even for observations that lie decades apart. V358 Aqr possesses an accreting pole in the upper hemisphere of the white dwarf that is visible over the entire orbital period of 209.45 min. The magnetic field strength derived from cyclotron line emission is 31.8 MG. The orbital motion of the cyclotron lines yields an inclination of 60° and an offset of the magnetic pole from the rotational axis of about 10°. The secondary star is of spectral type dM4.0 ± 0.5 and the distance is 540 ± 100 pc. V358 Aqr is peculiar in showing giant optical outbursts that bear all of the characteristics of stellar flares. With two flares observed in 72 h on source, the flare frequency may be high. The total energy radiated in the flare of 28 November 2010 exceeded 10^{36} erg. While the flares clearly occur on the secondary star, it seems that they may or may not be connected with coronal mass ejection and subsequent accretion onto the white dwarf.

Key words. novae, cataclysmic variables – stars: magnetic field – binaries: close – stars: flare – stars: individual: V358 Aquarii – X-rays: binaries

1. Introduction

The optical identification of X-ray sources from the ROSAT All Sky Survey (RASS; Trümper 1993; Voges et al. 1999; Boller et al. 2016) led to a boost in the knowledge of objects characterized by high-temperature plasma emissions; among these were polars, a subtype of magnetic semidetached close binaries. The present target, V358 Aqr = RX J2316-0527, is a long-period polar with $P_{\rm orb}$ = 3.48 h (Beuermann & Thomas 1993; Thomas et al. 1998). In the only other previous publication on this object, Rodrigues et al. (2006) derived an ephemeris and proved the magnetic nature of the white dwarf (WD) by the detection of circularly polarized cyclotron radiation. We present here a synopsis of results on V358 Aqr that we obtained over more than 25 yr.

V358 Aqr differs from most other polars by the occurrence of giant flares on the secondary star, which are of a type that have previously been detected in the prototype polar AM Her, although only on rare occasions: Shakhovskoy et al. (1993) and Saar et al. (2006, 2007) described one optical and one far ultraviolet (FUV) flare, respectively, while Kafka et al. (2005) did not detect a single similarly large optical flare in 13 yr of RoboScope coverage. In V358 Aqr, on the other hand, we detected two giant flares in a total of 72 h of observation time, suggesting a particularly active companion to the WD. This is of interest in the context of increasing evidence that active secondary stars in close binaries are surrounded by extended and complex magnetospheres with large-scale long-lived prominences. Such loop structures were discovered in AM Her (Staude et al. 2004; Kafka et al. 2006) and in the pre-cataclysmic binary QS Vir (Parsons et al. 2016). Low-level activity and mass-transfer variations have been detected in many polars. In the framework of the Roche-lobe overflow model, they may be connected to star-spot related activity in the vicinity of the inner Lagrangian (L1) point (Hessman et al. 2000). On the other hand, explosive events caused by the breakup of magnetic loops away from L1 could lead to mass transfer with characteristics different from Roche-lobe overflow (Staude et al. 2004). We do not yet have conclusive evidence for such events primarily because simultaneous optical or ultraviolet and X-ray coverage is lacking, but V358 Aqr is a comparatively bright X-ray source and appropriate coordinated observations may be instrumental in studying such a mode of mass transfer.

V358 Aqr is highly variable on long and short timescales with orbital mean magnitudes ranging from V = 15.8 to 18.6. The long-term variability is characterized by high and low states of accretion, with a living V-band light curve available from the Catalina Sky Survey monitoring program of "Ritter CVs" (Drake et al. 2009)[1]. The short-term variability outside the occasional flares is dominated by blue flickering, which is almost absent in low and intermediate states and becomes prominent in the high state.

⋆ Deceased 18 January 2012.

[1] http://nesssi.cacr.caltech.edu/catalina/CVservice/CVtable.html, where V358 Aqr is listed as Name = J2316-05 and Alt name = Aqr 5.

Table 1. ROSAT X-ray observations.

Dates	Type	Band	Exp. (s)	Total time	Accretion state
30 Nov.–2 Dec. 1990	X-ray	0.1 − 2.0 keV	~23	451 s	high ?
25–26 May 1993	X-ray	0.1 − 2.0 keV		4.3 h	low

Table 2. Spectroscopy with the MPG/ESO 2.2 m telescope equipped with EFOSC2 as detector.

Dates	Band (Å)	Resol. (Å)	Number	Expos. (min)	Total time	State
4 Sep. 1991	3491–5452	8	20	10	4.0 h	moderately
5 Sep. 1991	3200–8975	25	14	7	2.1 h	high
11 Nov. 1995	3800–9120	25	1	20	0.4 h	intermediate
29 Nov. 1995	3800–9120	25	8/7	18/5	3.3 h	intermediate

Table 3. Optical photometry with the ESO / Dutch 0.9 m telescope (1); the MONET/North telescope (2); and the MONET/South telescope (3).

Dates	Tel.	Band	Expos. (s)	Total time	State
23–26 Sep. 1998	(1)	*BVRI*	30/40	23.7 h	high
28 Nov.–29 Dec. 2010	(2)	WL	30/60	12.0 h	intermediate
29 Oct. 2011	(2)	WL	30	4.0 h	intermediate
11 Sep.–10 Nov. 2014	(2)	WL	60/120	15.7 h	intermediate
19 Jun.–7 Jul. 2016	(3)	WL	60	6.5 h	intermediate

2. Observations

V358 Aqr, which is located at RA(2000) = $23^h16^m03\overset{s}{.}6$, Dec(2000) = $-05°27'09''$ (l, b = 72.3, −58.6), was discovered as a bright very soft X-ray source in the RASS (Boller et al. 2016)[2]. We subsequently identified it spectroscopically as a long-period polar (Beuermann & Thomas 1993; Thomas et al. 1998). When reobserved in the ROSAT pointed mode in May 1993, it had lapsed into a low state (Table 1). No other X-ray observation of V358 Aqr is listed in the NASA HEASARC Archive[3].

Follow-up time-resolved spectrophotometric observations were performed in 1991 and 1995, using the ESO/MPG 2.2 m telescope equipped with EFOSC2. Grisms G1 and G3 yielded low- and medium-resolution spectra with FWHM resolutions of 25 Å and 8 Å, covering the entire optical band and the blue band, respectively. Table 2 lists the wavelength ranges, number of spectra, exposure times, and total times spent on source.

Time-resolved photometry was acquired in September 1998 and in several observing seasons between 2010 and 2016 (Table 3). All images were corrected for dark current and flat-fielded in the usual way. The spectrophotometry was wavelength calibrated, using He-Ar spectra, and flux calibrated, using spectra of standard stars; both of these were taken along with the target spectra. A total of 24 h of *BVRI* photometry of V358 Aqr was obtained in September 1998 with the ESO/Dutch 0.9 m telescope, when the source was in a high state of accretion, reaching V = 15.2. Exposure times ranged from 20 to 60 s. Relative photometry was performed with respect to the star SDSS J231600.10–052623.4, which is located 53″ W and 25″ N of V358 Aqr and has Sloan AB magnitudes u = 16.31, g = 14.61, r = 14.05, i = 13.86, and z = 13.81. Using the equations of Lupton (2005)[4], these numbers can be transformed to standard magnitudes B = 15.04(3), V = 14.23(3), R_c = 13.85(3) and I_c = 13.44(1), indicating a spectral type K0 or K1. Another 38 h of white-light (WL) photometry was acquired between 2010 and 2016 with the MONET/North and MONET/South telescopes[5] at the McDonald Observatory and the South African Astrophysical Observatory, respectively. In these observations, V358 Aqr was encountered in intermediate states, which were generally fainter by 2–3 mag than in 1998, except for a flare encountered on 28 November 2010. Exposure times were 30 or 60 s. Relative photometry was performed with respect to the star SDSS J231557.54-052658.1, which is located 90″ W and 11″ N of V358 Aqr and has Sloan AB magnitudes g = 17.43, r = 16.64, i = 16.32, and z = 16.16. The SDSS catalog quotes a dereddened r = 16.56. Its spectral type is K3 and its effective temperature $T_{\rm eff} \simeq 4600$ K.

We interpret the WL relative flux measurements with the help of synthetic photometry that models the overall throughput of the MONET telescopes (see Appendix). A WL AB magnitude w is defined analogous to the *ugriz* magnitudes. The pivot wavelength of the WL band, $\lambda_{\rm piv}$ = 6379 Å, falls in the Sloan r band and, not surprisingly, w agrees most closely with r, with a deviation of typically less than 0.10 mag for a wide range of incident spectra. We equate unity relative WL flux with respect to SDSS J231557.54-052658.1, therefore, with $w \simeq r$ = 16.6. In the Appendix, we quote selected colors for incident blackbody and power-law spectra.

3. Results

3.1. X-ray observations

V358 Aqr was observed in the RASS during 20 satellite passes between 30 November and 2 December 1990 with an average exposure time of 22.6 s. The bottom left panel of Fig. 1 shows the orbital light curve, which reaches up to 4 PSPC cts/s. The mean bright-phase count rate for the orbital phase interval ϕ = 0.2–0.8 is 1.8 cts s^{-1} (see Sect. 3.3 for the phase convention). The X-ray spectrum is characterized by a hardness ratio HR1 = −0.89 ± 0.02, implying that nearly all photons have energies below 0.4 keV (Boller et al. 2016)[6]. The mean soft RASS X-ray spectrum can be fitted with a single blackbody of temperature $kT_{\rm bb} \simeq 39$ eV, which is absorbed by a column density of neutral hydrogen $N_{\rm H} \simeq 4.5 \times 10^{20}$ H-atoms cm^{-2}, albeit with large mutually dependent errors. The bolometric flux of the soft X-ray component is $f_{\rm bb,bol} \simeq 10^{-10}$ erg cm^{-2} s^{-1}. With a small contribution from the hard component, the X-ray luminosity is $L_{\rm X} \simeq 4 \times 10^{33}$ erg s^{-1} for radiation into 4π and a distance of 540 pc (see Sect. 3.8). The optical magnitude of V358 Aqr at the time of the RASS is not known, but it was presumably in an intermediate or high state.

[2] http://cdsarc.u-strasbg.fr/viz-bin/qcat?J/A+A/588/A103

[3] http://heasarc.gsfc.nasa.gov/docs/archive.html

[4] https://www.sdss3.org/dr8/algorithms/sdssUBVRITransform.php

[5] https://monet.uni-goettingen.de

[6] http://cdsarc.u-strasbg.fr/viz-bin/qcat?J/A+A/588/A103. The hardness ratio HR1 = $(H - S)/(H + S)$, where H and S are the count rates in the 0.5–2.0 keV and the 0.1–0.4 keV bands, respectively.

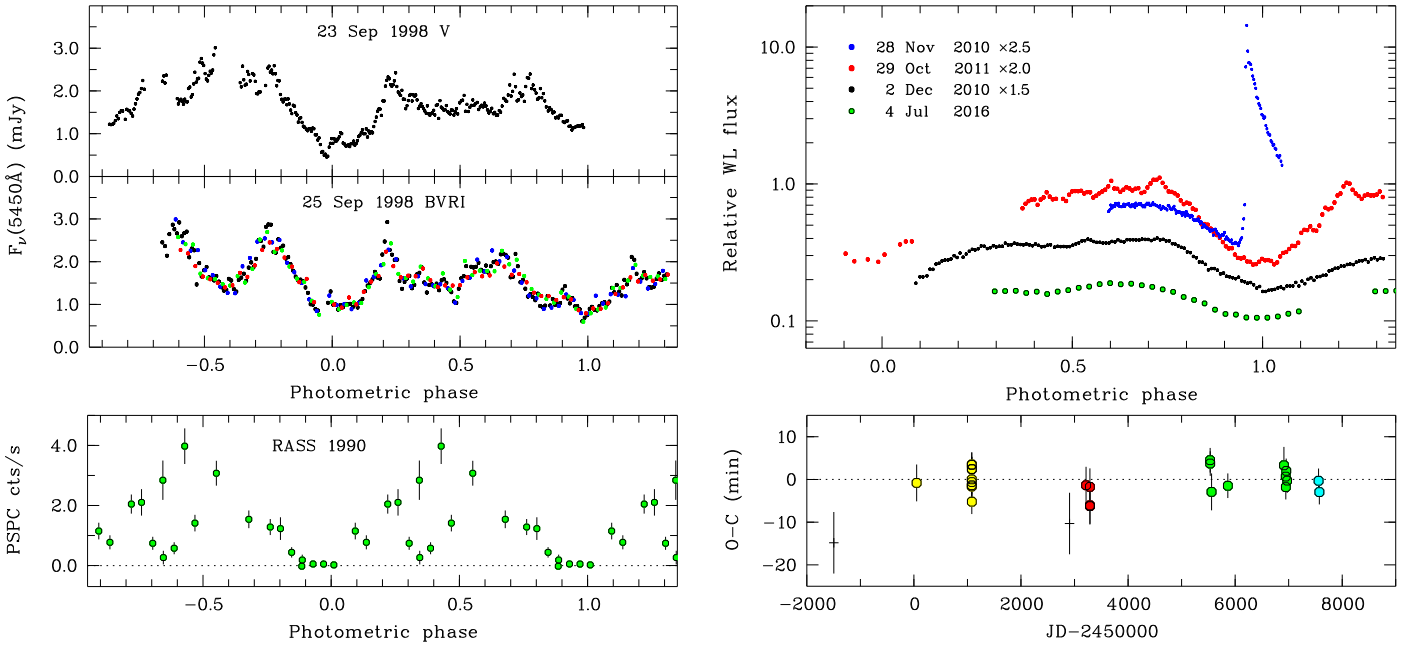

Fig. 1. *Bottom left*: soft X-ray light curve of V358 Aqr observed during the RASS in December 1990. *Top left*: high-state V-band light curve of 23 September 1998 and *BVRI* light curves of 25 September 1998 reduced to V, using the mean colors. *Top right*: intermediate-state light curves measured in WL in 2010, 2011, and 2016, shifted vertically to avoid overlap. *Bottom right*: O–C diagram, displaying the deviations of the times of the primary photometric minimum from the linear ephemeris of Eq. (1). The two data points indicated by crosses have been excluded from the linear fit that yields the ephemeris.

In a pointed ROSAT PSPC observation on 25 May 1993, the source was found in a low state with an average count rate of 0.009 cts s^{-1} and a hard X-ray spectrum. The light curve of that observation is consistent with that in Fig. 1, with an interval of low, but nonzero flux near $\phi \simeq 0$ and a finite flux near $\phi \simeq 0.5$.

3.2. Optical light curves

The top left panel of Fig. 1 shows *BVRI* light curves obtained in the September 1998 high state. A continuous train of 30 s V-band exposures was acquired on 23 September, while photometry on 25 September was performed in four filters with a sequence *VBVRVI*. The colors were remarkably constant, both through flares and as a function of orbital phase, $B-V = 0.12$, $V-R = 0.13$, and indicate a roughly flat spectral energy distribution (SED) $F_\nu = \text{const}$ over the wavelength range 4000–9000 Å or a blackbody of 12 000 K. Using the mean colors, we reduced the B, R, and I band measurements to the V band. The resulting light curve is shown in the second panel from the top (blue B, black V, green R, and red I). Maxima in the orbital light curves tended to occur near orbital phases $\phi = 0.25$ and $\phi = 0.75$, based on the ephemeris for the orbital minima quoted in Eq. (1), below. Flaring persisted at all orbital phases, complicating the measurement of the minimum times in some light curves. On 23 and 25 September 1998, V358 Aqr reached a peak V-band flux of 3.0 mJy ($V = 15.2$). The average bright-phase flux for the interval $\phi = 0.2$–0.8 was 2.2 mJy ($V = 15.5$). V358 Aqr was encountered about 3 mag fainter in a series of WL measurements taken between 2010 and 2016, with a mean bright-phase magnitude $w \simeq r = 17.5$ on 2 December 2010 and 18.4 on 4 July 2016, dropping to 19.0 in the orbital minimum (Fig. 1, top right panel). Flaring was much reduced or absent in these observations and the primary minimum was better defined than in the 1998 data, but some jitter persisted.

A notable exception from this general behavior was encountered on 28 November 2010, when the descent into primary minimum was interrupted by a giant flare that started at $\phi = 0.95$. This flare showed all signatures of a stellar flare on the secondary star (e.g., Kowalski et al. 2013), a pre-flare rise over a few minutes, an impulsive phase that lasted 100 s and included a rapid rise and similarly rapid decline, followed by a relaxation phase with an exponential decay time slowly increasing from 6 min to 12 min, over the 20 min coverage of the flare (Fig. 1, top right, and Fig. 5, upper left). In the 30 s exposures, the peak relative WL flux was 5.75, which corresponds to a peak r-band flux of 4.7 mJy and $V \simeq 14.6$, exceeding the 1998 high-state peak magnitude by 0.6 mag. Relative to the secondary star with $V = 20.5$ (Sect. 3.7), the flare amplitude amounted to 5.9 mag. Because of the blue SED of the flare (Fig. 4, lower right) and the rapid flux decrease of the secondary star at shorter wavelengths, the flare amplitude in the U band, which is usually quoted in discussions of stellar flares, may have exceeded 8 mag.

3.3. Orbital ephemeris

We determined the times of the photometric minima by the bisected-chord technique, which measures the midpoints of chords joining the ingress and egress curves. Our data set consists of 23 minima of our own, supplemented by five minima redetermined from the light curves of Rodrigues et al. (2006), all listed in Table 4. There is no systematic difference between the timings at different accretion levels, although the flickering in the 1998 high state extended through the minimum, complicating the timing. Such variability may also be responsible for the fact that the minimum in the 1991 spectrophotometry (Fig. 2) occurred 14.8 min early. Since there is no second minimum for comparison in the short 1991 run, we opted to exclude this timing from the period analysis. We also excluded one of the Rodrigues timings from the periodogram analysis because the

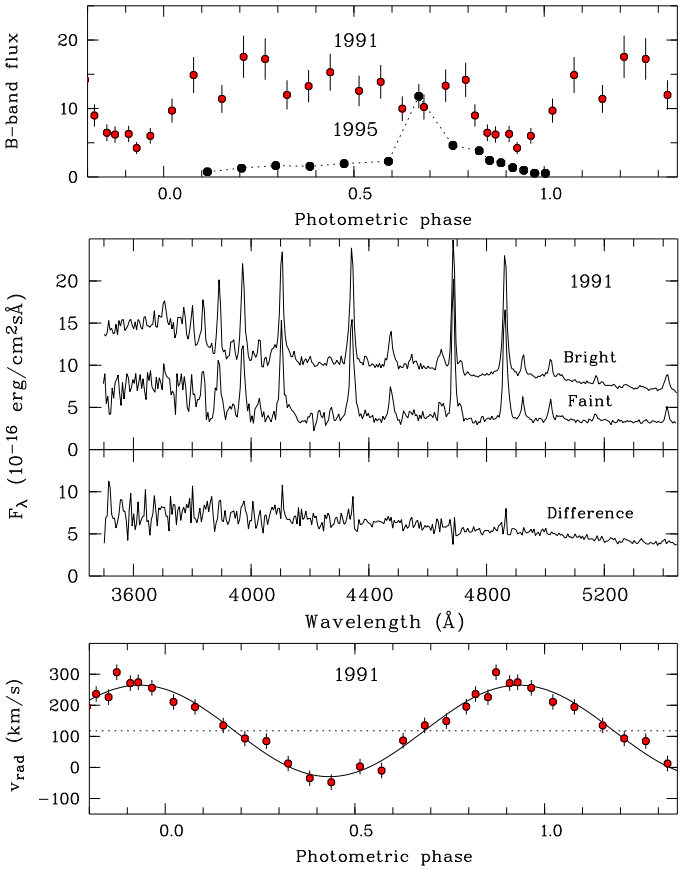

Fig. 2. *Top*: quasi-*B* band light curve of V358 Aqr in the 1991 high state (red) and in the 1995 intermediate state with a flare occurring in spectrum #7 (black). The ordinate is in units of 10^{-16} ergs cm^{-2} s^{-1} Å^{-1}. *Center*: mean spectra of the 1991 data for the bright and faint phase orbital intervals, 0.05–0.80 and 0.83–0.00, respectively, and the difference spectrum. *Bottom*: mean radial velocity variation in 1991 measured from single-Gaussian fits to the Hβ and HeIIλ4686 emission lines.

Table 4. Observed times of the primary minimum of V358 Aqr.

Cycle	BJD(TDB) 2 400 000+	Error (d)	Weight	O–C (min)	Ref.
−48 325	48 503.79740	0.00500	0	−14.82	1
−37 690	50 050.66540	0.00300	1	−0.81	1
−30 615	51 079.72542	0.00200	1	3.39	2
−30 608	51 080.74122	0.00200	1	0.01	2
−30 608	51 080.74008	0.00200	1	−1.63	2
−30 608	51 080.74028	0.00200	1	−1.34	2
−30 602	51 081.61349	0.00200	1	−0.60	2
−30 602	51 081.61558	0.00200	1	2.40	2
−30 602	51 081.61560	0.00200	1	2.43	2
−30 602	51 081.61634	0.00200	1	3.50	2
−30 601	51 081.75574	0.00200	1	−5.21	2
−29 972	51 173.24726	0.00110	1	−0.00	2
−18 047	52 907.72857	0.00500	0	−10.31	3
−15 929	53 215.79740	0.00300	1	−1.35	3
−15 442	53 286.63117	0.00300	1	−1.73	3
−15 435	53 287.64619	0.00300	1	−6.24	3
−15 429	53 288.51900	0.00300	1	−6.07	3
0	55 532.67080	0.00200	1	4.50	4
13	55 534.56111	0.00200	1	3.73	4
185	55 559.57386	0.00300	1	−2.91	4
2276	55 863.71032	0.00200	1	−1.47	4
9482	56 911.82466	0.00300	1	3.31	4
9716	56 945.85807	0.00200	1	0.67	4
9723	56 946.87451	0.00200	1	−1.79	4
9777	56 954.73144	0.00200	1	2.01	4
9894	56 971.74748	0.00200	1	−0.28	4
13 929	57 558.63726	0.00200	1	−0.31	5
14 032	57 573.61675	0.00200	1	−2.96	5

Notes. (1) MPI/ESO 2.2 m, spectrophotometry; (2) ESO/Dutch 0.9 m, photometry; (3) Rodrigues et al. (2006), reanalysis of original data; (4) MONET/N, photometry; (5) MONET/S, photometry.

corresponding light curve displays a flat-bottomed minimum of 45 min duration. This leaves us with 26 accepted minimum times that define $\phi = 0$. After conversion from UTC to Barycentric Dynamical Time (TDB; Eastman et al. 2010)[7], a least-squares fit yields the linear ephemeris

$$T_{\rm min} = {\rm BJD(TDB)}\ 2\,455\,532.66768(51) + 0.145449767(22)\,E, \quad (1)$$

which is free of cycle count errors and allows to correctly phase events around the orbit even for observations that lie decades apart. Figure 1 (bottom right panel) shows the O–C diagram. The rms O–C scatter of the 26 accepted timings amounts to 2.9 min or 0.014 phase units. Including the two discarded timings would not change this uniqueness.

3.4. Time-resolved spectrophotometry 1991

We obtained 1.2 orbits of medium-resolution spectrophotometry on 4 September 1991 and 0.6 orbits of low-resolution data on September 5 (Table 2). V358 Aqr was in an intermediate state with $V = 16.5 - 18.0$ and mean colors $B - V = -0.01$ and $U - B = -0.67$. The *B*-band light curve obtained on 4 September is displayed in the top panel of Fig. 2 (red filled circles). The second panel from the top shows the straight mean spectra (not corrected for radial-velocity shifts), separately for the bright and faint orbital intervals, $\phi = 0.05$–0.80 and $\phi = 0.83$–0.00, respectively. This is the light curve in which the primary minimum appeared 14.8 min early. No additional phasing information was obtained from the incomplete orbit measured on 5 September.

The emission lines are single-peaked with wings extending to 2000 km s^{-1}. The orbital velocity variation is quasi-sinusoidal with an amplitude that is largest at the base of the lines. No further internal structure is detectable. In particular, a narrow component is not clearly discernible at our spectral resolution of 8 Å FWHM. In other polars, such a component is associated with emission from the irradiated face of the secondary star. We take the observed line profiles as representative of the "broad" component, reflecting the streaming motion of the accreted plasma. For simplicity, we measure the radial velocities by fitting single Gaussians to the Hβ and HeIIλ4686 lines. The bottom panel of Fig. 2 shows the mean velocity variation of the two lines with an amplitude of 273 km s^{-1}. The orbital phase of peak positive radial velocity agrees with that of the spectrophotometric minimum and roughly with that of the X-ray minimum. We interprete primary photometric minimum as the closest approach of the line of sight to the accreting field line. Although the X-ray source is best in view at this phase, the fact that the X-ray flux

[7] http://astroutils.astronomy.ohio-state.edu/time/

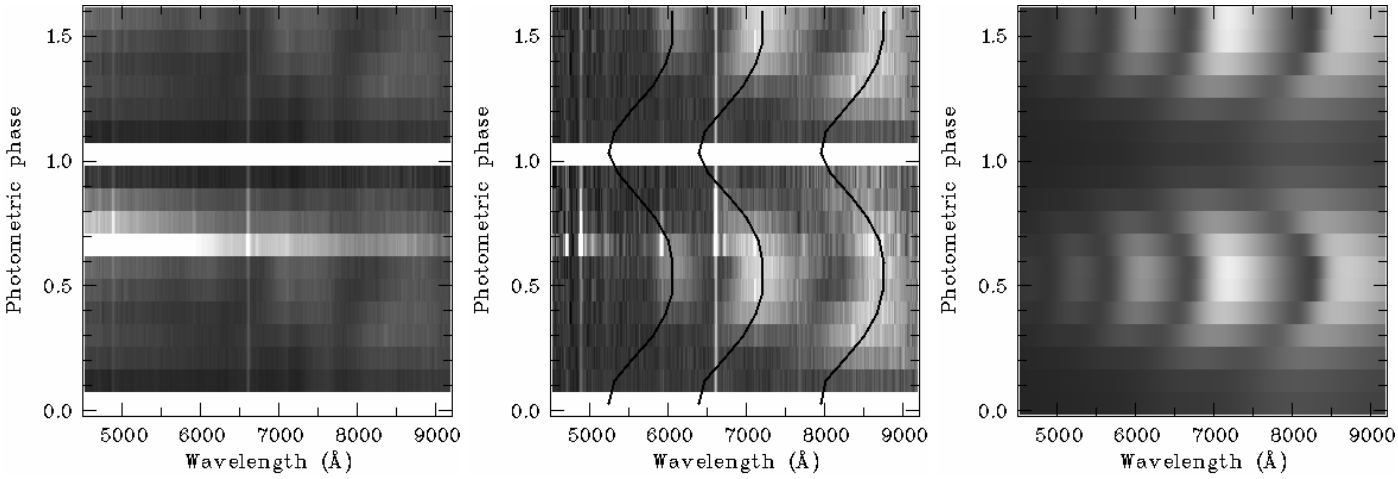

Fig. 3. Gray-scale representation of the low-resolution spectrophotometry of 29 November 1995 collected into 11 phase bins and repeated for 1.64 orbits. *Left*: observed spectra with the bin containing $\phi = 0$ remaining empty. *Center*: cyclotron spectra obtained by subtracting the dM4e secondary star and the underlying continuum. *Right*: model of the cyclotron line emission for a field strength of 31.8 MG (see text).

nevertheless assumes a minimum around $\phi = 0$ may be due to photoabsorption in a wide and dense accretion stream or curtain.

The emission lines and the associated Paschen and Balmer continuum originate in the accretion stream. This component displays little orbital variation in V358 Aqr and the difference between the bright-phase and faint-phase spectra is found to be an almost pure continuum (Fig. 2, third panel from the top). This component is best explained by optically thick cyclotron radiation and by the same token the orbital minimum is caused by cyclotron beaming (Fig. 1, upper right panel). The light curve is flat around $\phi = 0.5$, suggesting that the accreting pole stays in view all the time.

3.5. Time-resolved spectrophotometry 1995

Nearly a full orbit of low-resolution spectrophotometry was obtained on 29 November 1995, when the source was in an intermediate state of accretion with visual magnitude varying between 19.5 and 18.2, except for a flare that reached $V = 16.7$, averaged over the 18 min exposure time. The left panel in Fig. 3 shows a gray-scale representation of the spectra, in which the shorter exposed post-flare spectra (Table 2) were combined into two spectra with an equivalent exposure time of ∼18 min ($\Delta\phi = 0.091$). Of the 11 phase bins per orbit, the bin that contains $\phi = 0$ was not covered. The flux level of the first six spectra was about an order of magnitude fainter than in 1991 until a short-lived flux increase to the 1991 high-state level took place in spectrum #7 at $\phi \simeq 0.65$, followed by a decay on a timescale of ∼15 min (Fig. 2, top panel, black filled circles). Figure 4 (upper left panel) shows the evolution of the spectral flux through the event, indicated by the row numbers in Fig. 3: spectrum #1 centered on $\phi = 0.12$, the flare spectrum #7, and the spectra #8 and #9 of the relaxation phase. For comparison, we added the remarkably similar mean bright-phase spectrum of the 1991 high-state (red curve). Both spectra display similar blue continua with some difference in the strength of the Balmer jump and almost identical weak cyclotron lines in their red parts.

We corrected the 1995 spectra for interstellar extinction, using the total $A_V = 0.12$ at the position of V358 Aqr, justified by its large distance from the galactic plane (Sect. 3.8). The flare component was obtained by subtracting the mean of spectra #4 and #5 from spectrum #7, largely removing the secondary star, the cyclotron lines, and any other underlying spectral component. Figure 4 (lower right) shows the dereddened flare spectrum, fitted with a 13 000 K blackbody. The visual magnitude of the flare spectrum is $V = 16.9$. We return to the discussion in Sect. 3.9.

3.6. Cyclotron line emission

The 1995 phase-resolved spectra show moving cyclotron lines (left panel of Fig. 3). For further analysis, we subtracted a smooth continuum from each spectrum, resulting in the set of broad cyclotron lines and narrow atomic lines shown in the center panel. The flare that commences in spectrum #7 has no detectable influence on the strength of the cyclotron lines.

Model cyclotron spectra were calculated for an isothermal plasma with temperature kT and thickness parameter Λ in a magnetic field of strength B for an angle Θ between line of sight and field direction (Chanmugam & Dulk 1981). The observed spectrum is best defined, when the lines display their largest red shift (spectra #5 and #6). The mean of these two spectra and the best-fit isothermal model spectrum are shown in Fig. 4 (bottom left) as the black and red curve, respectively. The observed cyclotron lines are identified as the 4th to 7th harmonic (red numbers). The least-squares fit parameters are $B = 31.8 \pm 0.2$ MG, $kT = 9.5 \pm 1.0$ keV, $\log \Lambda = 3.5 \pm 0.2$, and $\Theta = 72\overset{\circ}{.}4 \pm 1\overset{\circ}{.}0$, with some interdependence of the errors. The phase-dependent motion of harmonics 5 and 6 in wavelength was least-squares fitted, using a parameterized form of the corresponding wavelengths for the optically thin case. Harmonic 4 was not included in the fit because it may no longer be optically thin. For simplicity, we assumed that the magnetic pole and the footprint of the field line lie on the same meridian. With the mean Θ for the two pre-flare spectra fixed at $72\overset{\circ}{.}4$, we find an inclination $i = 58\overset{\circ}{.}3$, an angle between the accreting field line and the rotational axis $\beta = 15\overset{\circ}{.}0$, and the phase of maximum redshift $\phi_0 = 0.55$. The viewing angle relative to the field line varies between $73\overset{\circ}{.}3$ and $43\overset{\circ}{.}3$, implying that the accreting pole is always in view. The fact that the Balmer lines in the 1991 medium-resolution spectra (Fig. 3) show large positive *and* negative radial velocities, although the viewing angle never exceeds 90°, may indicate the presence of a second hidden accretion region on the far hemisphere of the WD.

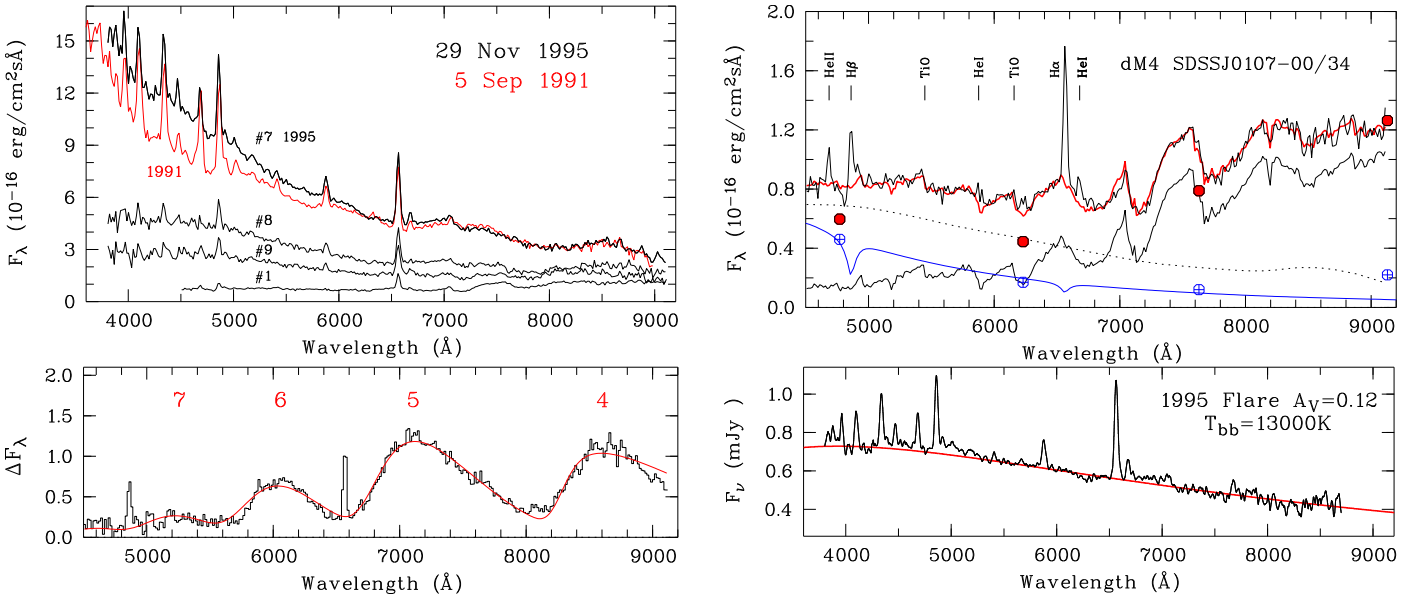

Fig. 4. *Top left*: flux-calibrated spectra #7, #8, #9, and #1 of the data of 29 November 1995 in Fig. 3 (black curves) and mean bright-phase spectrum of the 1991 high state (red curve). No extinction corrections have been applied. *Bottom left*: cyclotron spectrum measured at orbital phase $\phi = 0.53$, least-squares fitted with a model spectrum for an isothermal plasma of $kT = 9.5$ keV in a field of $B = 31.8$ MG (red curve). The numbers indicate the cyclotron harmonics. *Top right*: mean dereddened spectrum of 11 and 29 November 1995 near orbital minimum (upper solid black curve). Overplotted in red is the sum of the dM4e secondary (lower solid black curve) and a smooth underlying continuum (dotted black curve). Also shown is the SDSS *griz* photometry of 28 September 2009 (red filled circles), which can be represented by the secondary and a WD of 15 000 K (blue curve). *Bottom right*: dereddened flare spectrum and blackbody fit to the continuum.

Table 5. Synthesis of SDSS *griz* photometry of V358 Aqr of 28 September 2009.

Band	AB mag observed	AB mag dereddened	$F_{\lambda,\mathrm{dered}}$	$F_{\lambda,\mathrm{Sec}}$	$F_{\lambda,\mathrm{WD}}$	$F_{\lambda,\mathrm{Sec+WD}}$
			10^{-16} erg cm^{-2} s^{-1} Å^{-1}			
g	19.876(56)	19.734	0.597(12)	0.156	0.409	0.565
r	19.592(19)	19.489	0.445(10)	0.275	0.180	0.488
i	18.504(22)	18.426	0.789(11)	0.730	0.088	0.818
z	17.599(13)	17.544	1.263(24)	1.05	0.049	1.10

3.7. Stellar components

The spectral flux of the secondary star would be best derived from a spectrum taken at photometric minimum. The closest approach is provided by the first 18 min exposure of 29 November 1995, which covers the phase range $\phi = 0.08$–0.16, and a single 20 min spectrum of 11 November 1995, centered on $\phi = 0.95$. Both spectra show the same features of the secondary star superposed on an underlying blue continuum. The dereddened mean of the two is shown in Fig. 4 (upper right). We model this spectrum by the sum of an appropriate unreddened secondary star and a smooth continuum that accounts for the sum of the contributions by the white dwarf, cyclotron radiation, and the Paschen continuum of the stream emission. This method assigns all spectral structure (including the noise) to our representation of the secondary star. We employed a set of dereddened SDSS spectra of M dwarfs of spectral type dM3–dM5 (West et al. 2011). The best fit was obtained for the dM4.0 star SDSS J010730.81–000037.8 with its flux adjusted by a factor of 34 (lower black solid curve). The acceptable spectral type range is dM4.0 ± 0.5, which is in agreement with the spectral type expected from the evolutionary sequence of Knigge et al. (2011) for the orbital period of V358 Aqr. Our model spectrum (red curve) is the sum of the dM4 spectrum and the underlying continuum (dashed black curve). Model and data agree in all M-star features, including the TiO band heads at 5498 Å and at 6158 Å.

The SDSS *ugriz* photometric measurements of 28 September 2009 were performed at orbital phase 0.041–0.064, when V358 Aqr was in a deep low state. The dereddened *griz* fluxes are listed in Table 5 and are included as red filled circles in the upper right panel of Fig. 4. These fluxes are close to what might be expected from the stellar components alone. We fold our model of the secondary star with the *griz* filter response functions and subtract the derived fluxes from the 2009 SDSS fluxes. Of the residuals (symbols ⊕), g, r, and i are well matched by an adjusted 15 000 K WD spectrum (blue curve). The z band shows an excess flux that is possibly caused by remnant emission in the $n = 4$ cyclotron line. At the distance of 540 pc, the implied WD radius of 7.8×10^8 cm is that expected for a mass of 0.75 $M_\odot$, the standard mass in the Knigge et al. evolutionary sequence. Because of the uncertain mass, the temperature is only moderately constrained to 10 000–20 000 K.

3.8. Distance

We determine the distance of V358 Aqr from the dereddened spectral flux $f_{7500} = (0.87 \pm 0.10) \times 10^{-16}$ erg cm^{-2} s^{-1} Å^{-1} of the secondary at 7500 Å and the surface brightness F_{7500} $F_{7500} = (4.4 \pm 0.8) \times 10^5$ erg cm^{-2} s^{-1} Å^{-1} of a dM4.0 ± 0.5 star of near solar metalicity (Beuermann 2006). Lacking a mass measurement, we adopt $M_2 = 0.25\,M_\odot$, as quoted by Knigge et al. (2011) for an orbital period of 3.5 h. The radius of the Roche-lobe filling star then is $R_2 = 0.338\,R_\odot$. For a different secondary mass, R_2 varies as $M_2^{1/3}$. We can set approximate lower and upper limits to M_2 of 0.20 and 0.30 $M_\odot$, respectively. For evolutionary reasons, a long-period polar is not

expected to harbor a fully convective secondary with $M_2 < 0.20\,M_\odot$, while the radius of a main-sequence star with $M_2 > 0.30\,M_\odot$ quickly exceeds its Roche radius (Mann et al. 2015). With the above values of f_{7500} and F_{7500}, the distance is $d = R_2\,(F_{7500}/f_{7500})^{1/2} = (540\pm100)\,(M_2/0.25\,M_\odot)^{1/3}$ pc. At a galactic latitude of −58°.6, V358 Aqr is located below the galactic plane at $z = -460\,(M_2/0.25\,M_\odot)^{1/3}$ pc. It is plausible that most of the galactic gas and dust in this direction is located in front of the source.

3.9. Flare events of 1995 and 2010

The 2010 WL flare observed with 30 s time resolution displays all signatures of a stellar flare (e.g., Kowalski et al. 2013), a 1 min impulsive phase, followed by a relaxation phase with an exponential timescale that increases slowly from 6 to 12 min. We consider the 2010 and 1995 flares as a bona fide similar events that represent the temporal and spectroscopic flare evolution, respectively. We show that the temporal evolutions are consistent with being similar by extracting the flare component as the difference between the observed flux and underlying non-flare orbital flux variation. This operation is performed on the relative WL flux of the 2010 data and on the light curves in quasi-B, V, and R bands in the case of the 1995 spectrophotometry. For each band, the WL light curve of 29 October 2011 (Fig. 1), adjusted to the pre-flare phase bins, is used as a template for the underlying orbital variation. The resulting flare light curves in the B, V, and R bands are very similar with #8/#7 corrected flux ratios of 0.27, 0.32, and 0.28, respectively. The upper left panel of Fig. 5 shows the resulting relative WL flux versus time t, measured from the peak of the impulsive phase. Until $t = 19.4$ min, the histogram represents the observed data, beyond that the histogram is an extrapolation with the last measured exponential timescale. The upper right panel of Fig. 5 shows the mean BVR flux relative to that of bin #7 as the histogram, the very similar variation of the Hβ line flux as open circles, and the more rapidly decaying HeIIλ4686 line flux as asterisks. Averaging the 2010 flare light curve over 18 min exposures of the 1995 data and phase-shifting them, we find a flux ratio of two consecutive 18 min intervals of 0.28 if the flare peak occurs about 6 min into the first interval (histogram in the upper left panel), implying that the peak of the 1995 flare occurred about 6 min after the start of the #7 exposure, provided the temporal evolutions are, in fact, similar.

The average relative WL flux over the first 12 min of the 2010 flare of 1.95 corresponds to $r \simeq 16.6–2.5\log 1.95 \simeq 15.9$ and a mean r band flux of 1.62 mJy. The visual magnitude of the #7 flare spectrum in Fig. 4 (lower right panel) is $V = 16.9$. We account for the fact that only 12 min of the 18 min exposure cover the flare (factor 1.5) and use the colors in Table A.1 for $T_{\rm bb} = 13\,000$ K to arrive at a mean $r = 16.6$ for the first 12 min of the flare. Hence, on the assumption of a similar temporal evolution, the 2010 flare was brighter than that of 1995 by 0.7 mag and the luminosities and radiated energies differ by about a factor of two. We estimate the total energy E radiated in the 2010 flare, assuming blackbody emission from a time-independent emitting area $A = f\pi R_2^2$, with f the filling factor and $R_2 = 2.35\times10^{10}$ cm the radius of the secondary star. Then $E = A\int\sigma T_{\rm bb}(t)^4\,{\rm d}t$, with σ the Stefan-Boltzmann constant and $T_{\rm bb}$(t) the temperature at time t. Assuming that the 1995 blackbody temperature of 13 000 K is also valid for the first 12 min of the 2010 flare, the observed r band flux of 1.62 mJy is reproduced with a filling factor $f = 0.077$ and $A = 1.3\times10^{20}$ cm^2 at a distance of 540 pc. The peak flux of the impulsive phase of 4.7 mJy

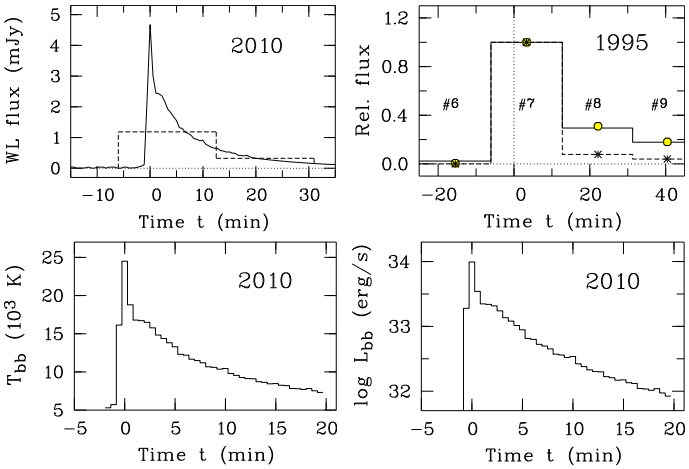

Fig. 5. *Top*: light curve of the 2010 flare component with 30 s exposures and ordinate in mJy (*left*) and relative flux of the 1995 flare component with 18 min exposures (*right*). *Bottom*: blackbody temperature through the 2010 flare (*left*) and blackbody luminosity (*right*), derived on the assumption of a time-independent emitting area.

implies a temperature $T_{\rm bb} \simeq 24500$ K and a peak luminosity of $L_{\rm bb} = 9.8\times10^{33}$ erg s^{-1}, the flux of 0.34 mJy at the end of the observation ($t = 19.4$ min) a temperature $T_{\rm bb} = 7300$ K and a luminosity $L_{\rm bb} = 8.4\times10^{31}$ erg s^{-1} (Fig. 5, bottom right). Performing the above integral yields a total energy $E = 1.2\times10^{36}$ erg radiated over the time interval from $t = -1.1$ min to $t = 19.4$ min. Up to 50% of this energy was released in the impulsive phase. The emitting area by far exceeds the cross section of the WD and the event originated undoubtedly on the secondary star. It represents one of the most luminous flares ever observed on a dM star. With a peak $V \simeq 14.7$ at a distance $d \simeq 540$ pc, the pure flare component reached an absolute visual magnitude $M_{\rm V} \simeq +6.0$. The 1995 flare displayed roughly similar energetics with a filling factor $f = 0.042$ for the same temperature structure. The fact that it showed no noticeable enhancement of the cyclotron line emission through the flare argues against accretion as a more than circumstantial energy source. The 1995 and the 2010 events occurred at different orbital phases in intermediate states of accretion. In a high accretion state, such an event would still be prominent if observed with sufficient time resolution.

3.10. Spectral energy distribution and accretion rate

Finally, it is instructive to consider the entire body of available brightness measurements collected into the SED $F_\nu(\lambda)$ in Fig. 6. The graph shows the spectrum of the 1991 high state and the sum of the secondary and WD spectra of Fig. 4 as the upper and lower solid curves, respectively. The photometric data from public archives were accessed via the Vizier SED tool provided by the Centre de Données astronomiques de Strasbourg (CDS)[8] and include the SDSS[9] (cyan blue dots), the Two Micron All Sky Survey (2MASS; Skrutskie et al. 2006, green dots), the Wide-field Infrared Survey (WISE; Cutri et al. 2013, magenta dot), the Galaxy Evolution Explorer (GALEX; Martin et al. 2005; Bianchi et al. 2011, blue dots), and the catalogs PPMXL (Roeser et al. 2010) and NOMAD (Zacharias et al. 2005) (crossed circles). The range of the MONET WL measurements of Fig. 1 is indicated by the three open triangles. The uppermost triangle refers to the level attained over a 100 s interval following

[8] http://vizier.u-strasbg.fr/vizier/sed/
[9] Data Release 13, http://www.sdss.org/dr13

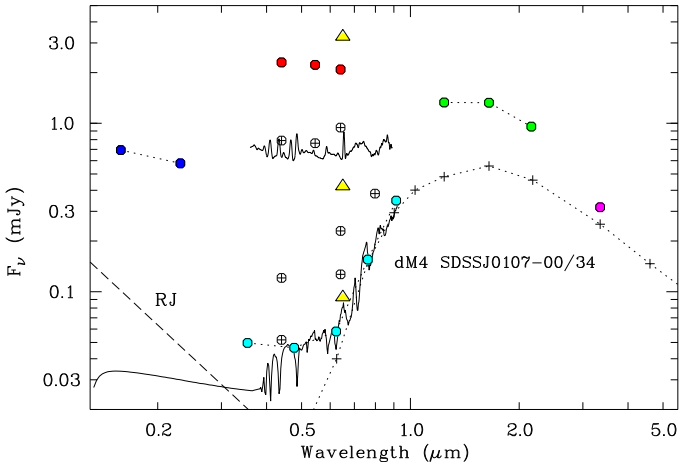

Fig. 6. Spectral energy distribution (SED) assembled from our own and archival data. It includes the 1991 spectrum and the sum of the secondary and WD spectra of Fig. 4 (top right and top left) as black curves the photometry of SDSS J010730.81-000037.8 adjusted by a factor of 34 (+) and photometry of our own and form public archives (see text).

the impulsive phase of the 2010 flare. The secondary star (+) represents a lower flux limit in the red part of the SED. The low-state SDSS fluxes in the *gri* bands agree with the sum of secondary and WD, but the *u* band flux exceeds the prediction. This excess requires either a WD that is hotter, smaller, and more massive than the adopted 0.75 $M_\odot$ WD or a hot pole cap, as found for example in the prototype polar AM Her also in its low state (Gänsicke et al. 2006). For illustrative purposes, we included a Raleigh-Jeans component (RJ; dashed line) that would account for the observed *u* band flux. The GALEX NUV and FUV points (blue) show that in the high state non-RJ components dominate the ultraviolet regime and emission from the accretion stream is a likely contender. The 2MASS fluxes (green) were also taken in a high state and contain a substantial contributions from the secondary star.

To a first approximation, the high state is characterized by a roughly flat SED from the infrared to the FUV, with $F_\nu \simeq 1$ mJy and an integrated energy flux of $F_{\rm UV,opt} \simeq 3\times10^{-11}$ erg cm^{-2} s^{-1}. At a distance of 540 pc, the UV/optical luminosity in an intermediate high state is $L_{\rm UV,opt} \simeq 1.0\times10^{33}$ erg s^{-1} for emission into 4π at a distance of 540 pc. The total X-ray flux measured in the RASS was $F_{\rm X} \simeq 10^{-10}$ erg cm^{-2} s^{-1} (Sect. 3.1), implying a total incident energy flux of $F_{\rm X,UV,opt} \simeq 1.3\times10^{-10}$ erg cm^{-2} s^{-1} and a luminosity $L_{\rm X,UV,opt} \simeq 5\times10^{33}$ erg s^{-1}. For a WD of 0.75 $M_\odot$, this luminosity requires an accretion rate $\dot{M} \simeq 4\times10^{16}$ g s^{-1} = 6×10^{-10} $M_\odot$ yr^{-1}, which is in the ball park of other long-period polars. In the exceptional 1998 high state, L and $\dot{M}$ may have been higher by at least another factor of two.

4. Discussion

With a period of 3.48 h, V358 Aqr is one of about 30 accepted long-period polars listed in the Ritter & Kolb (2003) catalog. Despite its distance of about 0.5 kpc, it reaches 15 mag in its high state with an accretion rate up to 10^{-9} $M_\odot$ yr^{-1}. The dM4 secondary is not far from being fully convective and the component masses, $M_2 \simeq 0.25\,M_\odot$ and $M_1 \simeq 0.75\,M_\odot$, are consistent with the predictions of the evolutionary sequence of Knigge et al. (2011). The field strength in the accretion spot on the upper hemisphere of the WD is 31.8 MG. The spot is permanently in view and the angle between the line of sight and the accreting field line never exceeds 90°. Nevertheless, the base of the emission lines extends to positive and negative radial velocities as high as 2000 km s^{-1}, which suggests that we may see plasma, streaming toward the visible pole and toward a second pole that is permanently hidden from view. These system parameters describe V358 Aqr as a perfectly normal long-period polar. The singular property that reveals V358 Aqr as a very peculiar system is the seemingly highly active secondary star, as evidenced by two giant flares observed in a total of only 72 h on source.

AM Her is the only other polar that has shown optical/UV outbursts of size and time structure similar to the 2010 event in V358 Aqr. These are rare events, however, Shakhovskoy et al. (1993) reported a large optical flare in AM Her and Saar et al. (2006, 2007) reported a flare in the FUV. Not a single event of similar size was seen in 13 yr of RoboScope coverage (Kafka et al. 2005). The 1992 flare of Shakhovskoy et al. (1993) was observed in *UBVRI* with simultaneous circular polarimetry. Based on the time structure of the flare, a color temperature of 12 000 K, an emitting area that exceeded the cross section of the WD, and the lack of detectable polarization, the flare was interpreted as having occurred on the secondary star with no mass being transferred to the WD. This was questioned by Bonnet-Bidaud et al. (2000), who would not exclude that dense matter was accreted that carried its kinetic energy to subphotospheric levels of the WD, avoiding noticeable circular polarization. In November 2003, Saar et al. (2006, 2007) observed part of a large FUV flare in AM Her, using the *Hubble* Space Telescope equipped with STIS. The energy radiated in the emission line CIVλ1550 amounted to $E_{\rm CIV} \sim 2.3\times10^{33}$ erg over 35 min and its radial velocity was consistent with an origin on the secondary star not far from the L_1 point. The SiIVλ1400 and HeIIλ1640 emission lines were also detected. The flare was accompanied by a strongly enhanced WD continuum that decayed faster then the CIV emission. It was characterized by a blackbody temperature $T_{\rm bb} \sim 10^5$ K, an emitting area $A \sim 2\times10^{16}$ cm^2, and a total energy release $E \sim 4\times10^{34}$ erg. The authors interpreted the event as a flare on the secondary star that was accompanied by coronal mass ejection (CME) and mass transfer to the WD. The events observed by Shakhovskoy et al. (1993) and Saar et al. (2006, 2007) seem to suggest that large flares on the secondary star may or may not be associated with CME and accretion of part of the matter.

An unequivocal signature of accretion would be the soft quasi-blackbody X-ray emission that is characteristic of many polars in their high states, but unfortunately neither the flare events observed in V358 Aqr nor the events of Shakhovskoy et al. (1993) and Saar et al. (2006, 2007) in AM Her had X-ray coverage. A hard X-ray flare was observed in UZ For (Pandel & Córdova 2002), but without simultaneous optical coverage. If V358 Aqr does, in fact, exhibit flares more frequently than other polars, a dedicated and coordinated campaign for simultaneous optical/X-ray coverage may shed light on a so far ill-understood accretion mode.

Acknowledgements. Much of the data analysis was performed by the late Hans-Christoph Thomas before his untimely death on 18 January 2012. We thank Claudia Rodrigues for sending us the original data of their published light curves of V358 Aqr. Our spectroscopic and photometric data were collected with the MPG/ESO 2.2 m and the ESO/Dutch 0.9 m telescopes at La Silla, Chile, and with the MONET/North and MONET/South telescopes of the MOnitoring NEtwork of Telescopes at the McDonald Observatory/Texas, and the SAAO at Sutherland, South Africa. The MONET telescopes were funded by the Alfried Krupp von Bohlen und Halbach Foundation and are operated by the Georg-August-Universität Göttingen, the McDonald Observatory of the University of Texas at Austin, and the South African Astronomical Observatory. In establishing the spectral energy distributions, we have used the Sloan Digital Sky Survey (SDSS),

the Two Micron All Sky Survey (2MASS), data obtained with the Wide-field Infrared Survey Explorer (WISE), and the NASA Galaxy Evolution Explorer (GALEX), accessed via the VizieR Photometric viewer operated at CDS, Strasbourg, France (http://vizier.u-strasbg.fr/vizier/sed/).

References

Beuermann, K. 2006, A&A, 460, 783
Beuermann, K., & Thomas, H.-C. 1993, Adv. Space Res., 13, 115
Bianchi, L., Efremova, B., Herald, J., et al. 2011, MNRAS, 411, 2770
Boller, T., Freyberg, M. J., Trümper, J., et al. 2016, A&A, 588, A103
Bonnet-Bidaud, J. M., Mouchet, M., Shakhovskoy, N. M., et al. 2000, A&A, 354, 1003
Chanmugam, G., & Dulk, G. A. 1981, ApJ, 244, 569
Cutri, R. M., Wright, E. L., Conrow, T., et al. 2013, Explanatory Supplement to the AllWISE Data Release Products, eds. R. M. Cutri et al., 1
Drake, A. J., Djorgovski, S. G., Mahabal, A., et al. 2009, ApJ, 696, 870
Eastman, J., Siverd, R., & Gaudi, B. S. 2010, PASP, 122, 935
Gänsicke, B. T., Long, K. S., Barstow, M. A., & Hubeny, I. 2006, ApJ, 639, 1039
Hessman, F. V., Gänsicke, B. T., & Mattei, J. A. 2000, A&A, 361, 952
Kafka, S., Robertson, J., Honeycutt, R. K., & Howell, S. B. 2005, AJ, 129, 2411
Kafka, S., Honeycutt, R. K., & Howell, S. B. 2006, AJ, 131, 2673
Knigge, C., Baraffe, I., & Patterson, J. 2011, ApJS, 194, 28
Kowalski, A. F., Hawley, S. L., Wisniewski, J. P., et al. 2013, ApJS, 207, 15
Mann, A. W., Feiden, G. A., Gaidos, E., Boyajian, T., & von Braun, K. 2015, ApJ, 804, 64
Martin, D. C., Fanson, J., Schiminovich, D., et al. 2005, ApJ, 619, L1
Pandel, D., & Córdova, F. A. 2002, MNRAS, 336, 1049
Parsons, S. G., Hill, C. A., Marsh, T. R., et al. 2016, MNRAS, 458, 2793
Ritter, H., & Kolb, U. 2003, A&A, 404, 301
Roeser, S., Demleitner, M., & Schilbach, E. 2010, AJ, 139, 2440
Rodrigues, C. V., Jablonski, F. J., D'Amico, F., et al. 2006, MNRAS, 369, 1972
Saar, S. H., Kashyap, V. L., & Ringwald, F. A. 2006, IAU Joint Discussion, 4, 30
Saar, S. H., Kashyap, V. L., & Ringwald, F. A. 2007, UV Astronomy: Stars from Birth to Death, 249
Schlegel, D. J., Finkbeiner, D. P., & Davis, M. 1998, ApJ, 500, 525
Shakhovskoy, N. M., Alexeev, I. Y., Andronov, I. L., & Kolesnikov, S. V. 1993, Cataclysmic Variables and Related Physics, Ann. Israel Phys. Soc., 10, 237
Skrutskie, M. F., et al. 2006, AJ, 131, 1163
Staude, A., Schwope, A. D., Hedelt, P., Rau, A., & Schwarz, R. 2004, Magnetic Cataclysmic Variables, IAU Colloq. 190, 315, 251
Thomas, H.-C., Beuermann, K., Reinsch, K., et al. 1998, A&A, 335, 467
Trümper, J. 1993, Science, 260, 1769
Voges, W., Aschenbach, B., Boller, T., et al. 1999, A&A, 349, 389
West, A. A., Morgan, D. P., Bochanski, J. J., et al. 2011, AJ, 141, 97
Zacharias, N., Monet, D. G., Levine, S. E., et al. 2005, VizieR Online Data Catalog: I/297

Appendix A: Synthetic photometry

We model the photon response of the MONET telescopes, considering the throughput of the telescope, the transmissions of the Bessell *UBVRI*, Sloan *ugriz*, and the CLEAR filter used for the WL measurements, the quantum efficiency of the detector, and the transmission of the atmosphere at an adopted airmass of 1.40 at 2000 m altitude. The overall photon response with the CLEAR filter extends from 4430 Å to 8430 Å at the 50% level. The pivot wavelength $\lambda_{\rm pivot}$ relates the mean fluxes by $\langle F_\nu\rangle = \langle F_\lambda\rangle\,\lambda^2_{\rm pivot}/c$, with c the speed of light. For the MONET WL band, $\lambda_{\rm pivot} = 6379$ Å falls in the Sloan r band. We define a WL AB magnitude w analogous to the *ugriz* AB magnitudes and calculate the standard *UBVRI* and *wugriz* AB magnitudes for normalized incident blackbody spectra with temperature $T_{\rm bb}$ and power law spectra $F_\nu \propto \nu^m$ with integer m. As expected, the color $w-r$ is least dependent on $T_{\rm bb}$ and m. Tables A.1 and A.2 list the results for selected colors.

The mean value of the color $w-r$ for the considered set of 12 spectra is $w-r = -0.032$ with a standard deviation of 0.078. Hence, the AB magnitude w corresponds closely to that of the Sloan r band, rather independent of the incident spectrum. Furthermore, the standard magnitude V is numerically close to the AB magnitude w. For instance, for an $F_\nu = $ const spectrum with zero AB colors, $V-w = -0.026$. The color transformations are naturally better defined if the incident spectrum is known.

Table A.1. Synthetic colors of blackbody spectra with temperature $T_{\rm bb}$.

$T_{\rm bb}$ (K)	4500	7000	10 000	13 000	18 000	25 000
$B-V$	0.920	0.421	0.163	0.033	−0.079	−0.154
$V-w$	0.242	−0.027	−0.105	−0.127	−0.136	−0.137
$w-g$	−0.666	−0.138	0.078	0.171	0.243	0.286
$w-r$	0.039	0.082	0.044	0.008	−0.032	−0.065
$w-i$	0.433	0.123	−0.091	−0.215	−0.331	−0.414

Table A.2. Synthetic colors of power-law spectra $F_\nu \propto \nu^m$.

m	−3	−2	−1	0	+1	+2
$B-V$	0.828	0.599	0.371	0.142	−0.086	−0.315
$V-w$	0.523	0.290	0.105	−0.026	−0.103	−0.126
$w-g$	−0.930	−0.571	−0.260	0.000	0.209	0.366
$w-r$	−0.184	−0.071	−0.009	0.000	−0.047	−0.149
$w-i$	0.499	0.386	0.220	0.000	−0.277	−0.610